A Hybrid Rectifier Mode Control for Communication-Free Wireless Power Transfer

Zhu, Gangwei; Dong, Jianning; Bauer, Pavol

DOI
10.1109/ECCE55643.2024.10861615

Publication date
2024

Document Version
Final published version

Published in
2024 IEEE Energy Conversion Congress and Exposition, ECCE 2024 - Proceedings

A Hybrid Rectifier Mode Control for Communication-Free Wireless Power Transfer

1st Gangwei Zhu
Department of Electrical Engineering, Mathematics and Computer Science
Delft University of Technology
Delft, the Netherlands
G.Zhu-2@tudelft.nl

2nd Jianning Dong
Department of Electrical Engineering, Mathematics and Computer Science
Delft University of Technology
Delft, the Netherlands
J.Dong-4@tudelft.nl

3th Pavol Bauer
Department of Electrical Engineering, Mathematics and Computer Science
Delft University of Technology
Delft, the Netherlands
P.Bauer@tudelft.nl

2024 IEEE Energy Conversion Congress and Exposition (ECCE) | 979-8-3503-7606-7/24/$31.00 ©2024 IEEE | DOI: 10.1109/ECCE55643.2024.10861615

***Abstract*—This paper presents a hybrid rectifier mode control for broad-range output power regulation in wireless power transfer (WPT) systems. The proposed control method employs a secondary-side active rectifier for output tuning, thereby eliminating the necessity for communication links. Furthermore, leveraging the pulse-skipping technique, two hybrid modes are introduced in the proposed approach. These hybrid modes reduce circulating reactive power within the resonant circuits, thereby optimizing the transmission efficiency of the WPT systems. To validate the effectiveness of the proposed method, experiments were conducted using a WPT prototype. Experimental results demonstrate that the proposed approach achieves higher efficiency than the conventional phase-shift control strategy, with a maximum efficiency improvement of up to 3.7%.**

***Index Terms*—Wireless power transfer, pulse-skipping technique, hybrid rectifier mode control, efficiency optimization**

I. Introduction

Wireless power transfer (WPT) technology offers a flexible and weather-proof solution for charging a variety of industrial devices, including portable electronics [1], [2], biomedical implants [3], [4], inspection robots [5], and electric mobility [6]–[9]. In these practical applications, the equivalent load of WPT systems often experiences significant variations. Consequently, to accommodate these load variations, it is imperative for WPT systems to achieve wide output power regulation [10].

One straightforward approach to achieving wide output power regulation involves cascading DC-DC converters at the front and back ends of the system [11]–[14]. Although this method enables broad output regulation, it introduces additional components and associated power losses.

Alternatively, implementing phase-shift control in the inverter and rectifier provides an effective means for achieving wide output power capability [15]–[17]. However, the phase-shift control technique results in hard switching under load variations, leading to reduced efficiency and potential electromagnetic interference (EMI) issues [18]. To achieve zero-voltage-switching (ZVS) under wide-range power variations, several control variables have been introduced in previous studies [19]–[23]. In [19], frequency tuning was implemented to facilitate wide ZVS. However, adjusting the frequency in WPT systems is susceptible to the bifurcation phenomenon [24]. When the bifurcation phenomenon occurs, the system operates in a severe detuning state, leading to substantially increased coil currents [25]. In contrast, the switch-controlled-capacitor (SCC) technique was utilized in [20]. Although wide-range ZVS can be achieved through dynamic SCC tuning, this method results in extra power switches. To avoid the bifurcation phenomenon and the need for extra power switches, a triple-phase-shift (TPS) control strategy was proposed in [21]. In the TPS control method, the phase difference between the inverter and rectifier AC voltages are tuned for wide-range ZVS. This method, however, results in substantial reactive power under load variations. Recently, based on the TPS approach, the half-bridge (HB) mode was further introduced to reduce reactive power and improve efficiency under light-load conditions [22], [23]. Nevertheless, the HB mode introduces DC-blocking voltages across the compensation capacitors, thus increasing their voltage stresses. Additionally, as the tuning range of the HB mode is limited, the reactive power is still considerable at some power levels.

To address the aforementioned challenges, this paper proposes a hybrid rectifier mode control to achieve wide output power regulation in WPT systems. The main advantages of the proposed method are summarized as follows:

1) The proposed method enables wide output power regulation without the need for additional DC-DC converters. Additionally, it requires no extra hardware circuits or components, making it straightforward to implement in existing active-rectifier-based WPT systems.

2) The proposed control technique adopts an active rectifier on the secondary side to realize output tuning, thereby obviating the requirement for dual-side communication.

3) The proposed approach introduces two hybrid modes for wide power regulation. These hybrid modes significantly reduce circulating reactive power within the resonant circuits, thereby enhancing the transmission efficiency of the system. Compared to the existing HB mode, the proposed hybrid mode control demonstrates significant advantages by effectively eliminating capacitor DC-blocking voltages and providing enhanced tuning flexibility.

The remainder of this paper is structured as follows: Section II presents the circuit topology and output power analysis of the investigated WPT system. Subsequently, Section III elu-

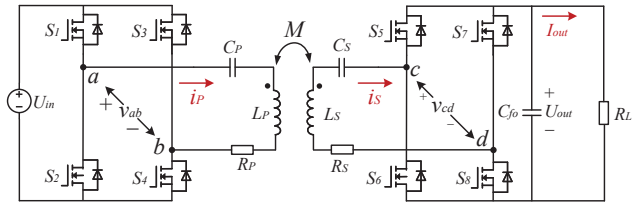

Fig. 1. Circuit topology of the investigated WPT system.

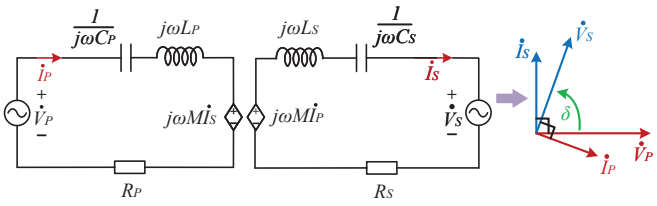

Fig. 2. Equivalent circuit model and phasor diagram of the investigated WPT system.

cidates the fundamental working principles of the secondary-side rectifier control. Furthermore, Section IV demonstrates the proposed hybrid rectifier mode control. Experimental results validating the proposed approach are then presented in Section V. Finally, conclusions are drawn in Section VI.

II. Circuit Topology and Output Power Analysis of the Investigated WPT System

A. Circuit Topology

Fig. 1 demonstrates the circuit topology of the investigated WPT system. In WPT systems, the contactless charging coils form a loosely coupled transformer due to the significant air gap between the transmitter (Tx) coil and the receiver (Rx) coil. To counteract the substantial leakage inductance caused by the loosely-coupled transformer, compensation capacitors are essential. This paper investigates the most commonly adopted series-series (SS) compensation topology as it offers advantages in ease of implementation and minimal passive components [26]. Moreover, to minimize the conduction losses of the rectifier, an active rectifier is employed to replace the conventional diode rectifier.

Additionally, the definitions of the symbols in Fig. 1 are elaborated as follows: U_{in} and U_{out} denote the DC input and output voltages of the system; v_{ab} and v_{cd} are the AC voltages excited by the inverter and active rectifier, respectively; i_P and i_S are the Tx and Rx coil currents; L_P and L_S indicate the self-inductances of the Tx and Rx coils, while M represent their mutual inductance; C_P and C_S are the compensation capacitors for L_P and L_S; R_P and R_S are the equivalent loss resistances of the primary and secondary resonant circuits; R_L is the equivalent load resistance; I_{out} is the DC output current flowing through R_L.

B. Output Power Analysis

According to the fundamental harmonic approximation (FHA) method, the equivalent circuit model and phasor diagram of the system are further illustrated in Fig. 2. Wherein, $\dot{V}_P$, $\dot{V}_S$, $\dot{I}_P$, and $\dot{I}_S$ represent the phasor forms of the fundamental components in v_{ab}, v_{cd}, i_P, and i_S, respectively; δ is the phase difference angle between $\dot{V}_P$ and $\dot{V}_S$; ω is the angular switching frequency.

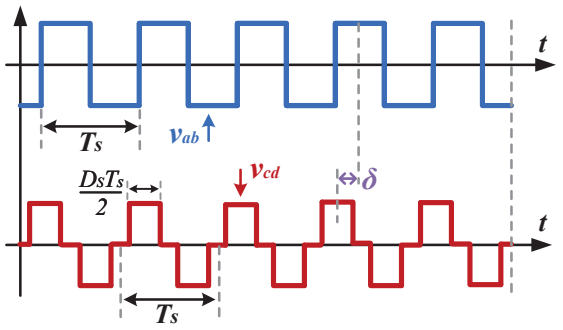

Fig. 3. Typical operating waveforms of the secondary-side rectifier control. Herein, T_s denotes the switching cycle of v_{ab} and v_{cd}, while $D_S (D_S \in [0, 1])$ represents the duty cycle of v_{cd}.

Based on the FHA model presented in Fig. 2, fundamental circuit equations of the system are given by

$$\begin{cases} \dot{V}_P &= (R_P + jX_P)\dot{I}_P - j\omega M\dot{I}_S, \\ \dot{V}_S &= j\omega M\dot{I}_P - (R_S + jX_S)\dot{I}_S, \end{cases} \tag{1}$$

where

$$\begin{cases} X_P &= \omega L_P - \dfrac{1}{\omega C_P}, \\ X_S &= \omega L_S - \dfrac{1}{\omega C_S}. \end{cases} \tag{2}$$

Following the Fourier series expansion, the RMS values of $\dot{V}_P$ and $\dot{V}_S$ are derived as

$$|\dot{V}_P| = G_{inv}U_{in}, |\dot{V}_S| = G_{rec}U_{out}, \tag{3}$$

where G_{inv} and G_{rec} are the DC to AC voltage gains of the inverter and rectifier, respectively.

Furthermore, assuming the primary and secondary resonant circuits are properly compensated and ignoring the loss resistances, the output power of the system (P_{out}) is derived as

$$P_{out} = G_{inv}G_{rec}\frac{U_{in}U_{out}}{\omega M}\sin(\delta). \tag{4}$$

As it can be observed from (4), the output power of the system can be regulated by tuning the DC to AC voltage gains of the inverter and rectifier (G_{inv} and G_{rec}).

III. Secondary-side Rectifier Control

In WPT systems, the inherent contactless nature between the primary and secondary sides often necessitates the use of a communication link. This link facilitates the transmission of load-side information from the secondary side to the primary side, enabling the regulation of the primary-side inverter for effective power control. However, this approach leads to significant communication latency and increased hardware

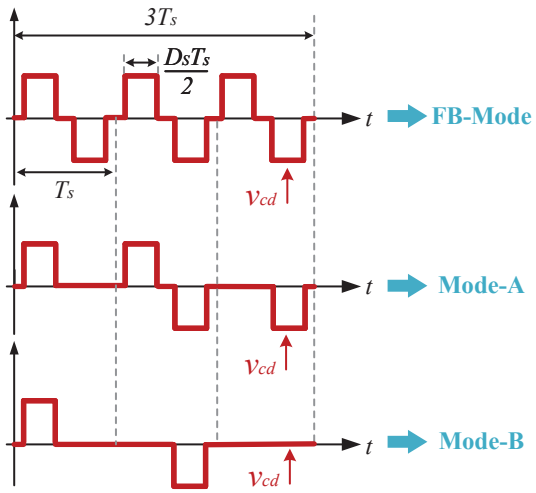

Fig. 4. Typical operating waveforms of the proposed hybrid rectifier modes. Herein, T_s denotes the switching cycle of v_{ab} and v_{cd}, while $D_S(D_S \in [0,1])$ represents the duty cycle of v_{cd}.

complexity [27]. Hence, it is preferable to eliminate the need for communication links in WPT systems.

To achieve communication-free power regulation, the proposed approach employs secondary-side rectifier control. Unlike conventional primary-side inverter control, secondary-side rectifier control enables output power tuning by regulating the secondary-side active rectifier, thereby obviating the need for communication links. Fig. 3 illustrates the typical operating waveforms of the secondary-side rectifier control. As it can be observed, the inverter output voltage (v_{ab}) remains fixed at an 85 kHz full-duty-cycle square wave in secondary-side rectifier control, and the inverter voltage gain is given by

$$G_{inv} = \frac{2\sqrt{2}}{\pi}. \tag{5}$$

In contrast, as shown in Fig. 3, the rectifier input voltage (v_{cd}) is dynamically tuned for output power regulation in secondary-side rectifier control. Specifically, the rectifier voltage gain under the conventional FB mode (G_{rec_FB}) is expressed as

$$G_{rec\_FB} = \frac{2\sqrt{2}}{\pi}\sin(\frac{D_S\pi}{2}), \tag{6}$$

where $D_S(D_S \in [0,1])$ indicates the duty cycle of v_{cd}.

According to the analysis in [28], a significant challenge of secondary-side rectifier control is the necessity for substantial reactive power to achieve ZVS under varying power levels. This considerable reactive power circulating within the resonant circuits consequently leads to a notable decline in efficiency as the output power varies.

IV. Proposed Hybrid Rectifier Mode Control

A. Hybrid Rectifier Mode

To minimize the circulating reactive power and enhance transmission efficiency, this paper introduces two novel hybrid modes, i.e., mode-A and mode-B, for rectifier modulation.

Typical operating waveforms of the proposed hybrid rectifier modes are illustrated in Fig. 4. As shown in Fig. 4, the proposed hybrid modes skip several pulses to deliver power under load variations. Specifically, mode-A skips two pulses within three switching cycles, while mode-B skips four pulses within the same period. Moreover, by symmetrically and homogeneously distributing the pulses, both the even-subharmonics and the DC component within the rectifier input voltage are removed. This reduces harmonic distortions in coil currents and eliminates DC-blocking voltage across capacitors.

Furthermore, applying the Fourier series expansion, the rectifier voltage gains under the proposed hybrid modes are derived as

$$\begin{cases} G_{rec\_MA} &= \frac{2}{3} \times \frac{2\sqrt{2}}{\pi}\sin(\frac{D_S\pi}{2}), \\ G_{rec\_MB} &= \frac{1}{3} \times \frac{2\sqrt{2}}{\pi}\sin(\frac{D_S\pi}{2}), \end{cases} \tag{7}$$

where G_{rec_MA} and G_{rec_MB} represent the rectifier voltage gains in the proposed mode-A and mode-B, respectively. As evident from (7), the pulse skipping technique contributes to a proportional reduction in the rectifier voltage gain. Consequently, as the output power decreases, the rectifier is able to transition from the conventional FB mode to mode-A and mode-B, facilitating efficient output regulation under load variations.

B. Implementation of ZVS

In high-frequency WPT systems, the implementation of ZVS is of great significance. According to the analysis in [23], to enable ZVS for both the inverter and rectifier while minimizing the reactive power, the phase difference angel δ needs to satisfy:

$$\delta = \min\{\frac{D_P\pi}{2}, \frac{D_S\pi}{2}\} - \delta_m, \tag{8}$$

where δ_m is the margin angle to ensure sufficient ZVS current for charging/discharging the equivalent output capacitance C_{oss} of the power switches. It is noteworthy that the inverter duty cycle D_P is maintained at $D_P = 1$ in the secondary-side rectifier control. Therefore, the following relationship is consistently satisfied: $D_P \geq D_S$.

Consequently, the ZVS criteria for the proposed method can be simplified as

$$\delta = \frac{D_S\pi}{2} - \delta_m. \tag{9}$$

C. Reduction of Circulating Reactive Power

Based on (4), (5), (6), (7), and (9), the variations in the rectifier duty cycle D_S and the phase difference angle δ in response to power fluctuations are demonstrated in Fig. 5. As shown in Fig. 5, the proposed method significantly reduces the tuning range of D_S and enhances the value of δ as the output power decreases.

According to [23], the circulating reactive power within the reasonant circuits (Q_{cir}) can be expressed as

$$Q_{cir} = -G_{inv}G_{rec}\frac{U_{in}U_{out}}{\omega M}\cos(\delta). \tag{10}$$

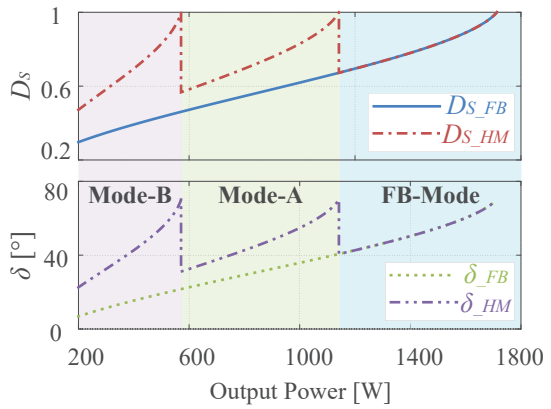

Fig. 5. Variations of the rectifier duty cycle D_S and the phase angle δ under varying power levels. Here, the subscript "FB" indicates the traditional FB mode, while "HM" represents the proposed hybrid modes.

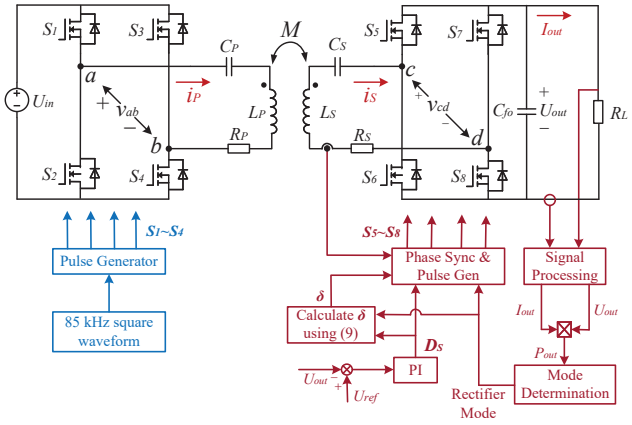

Fig. 6. Block diagram of the proposed hybrid rectifier mode control.

TABLE I
DETAILED ELECTRICAL SPECIFICATIONS OF THE DEVELOPED WPT PROTOTYPE

Symbol	Parameters	Value	Unit
M	Mutual inductance	78	μH
L_P	Self-inductance of Tx coil	335.8	μH
L_S	Self-inductance of Rx coil	220.0	μH
C_P	Primary compensation capacitance	10.6	nF
C_S	Secondary compensation capacitance	16.1	nF
U_{in}	DC input voltage	300	V
U_{out}	DC output voltage	300	V
f	Switching frequency	85	kHz

As evident from (10), a higher value of δ results in decreased circulating reactive power, consequently achieving improved efficiency [21]–[23].

D. Control Framework

Fig. 6 further demonstrates the framework of the proposed control approach. As illustrated in Fig. 6, the proposed method initially measures the DC output voltage and current to obtain the output power of the system (P_{out}). Subsequently, the measured P_{out} is fed to the mode determination module. As the output power diminishes, the rectifier mode transitions from the FB mode to mode-A and mode-B. Afterward, a PI controller is implemented to achieve reference voltage tracking by dynamically adjusting the rectifier duty cycle D_S. The phase difference angle δ, on the other hand, is regulated accordingly for the implementation of wide-range ZVS. Notably, the primary-side inverter is driven by an 85 kHz full-duty-cycle square wave signal, and there is no need for dual-side communication.

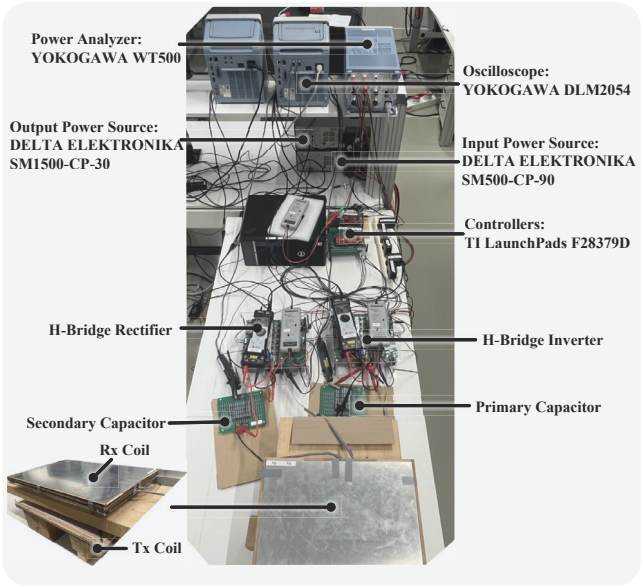

Fig. 7. Physical demonstration of the developed experimental prototype.

V. Experimental Results

A. Experimental Prototype

To validate the effectiveness of the proposed hybrid rectifier mode control, a WPT prototype was developed, as demonstrated in Fig. 7.

Within this prototype, a DC power supply (DELTA ELEKTRONIKA SM500-CP-90) was employed to provide the required power. On the other hand, another bidirectional DC source (DELTA ELEKTRONIKA SM1500-CP-30) was adopted as the electronic load. The operating waveforms were measured by an oscilloscope (YOKOGAWA DLM2054), while the DC-to-DC transmission efficiency of the system was measured by a power analyzer (YOKOGAWA WT500).

Moreover, two H-bridge converters were developed as the inverter and active rectifier, respectively. The control algorithm and PWM generation were implemented in TI LaunchPads F28379D. Further detailed electrical specifications of the developed experimental prototype are elaborated in Table I.

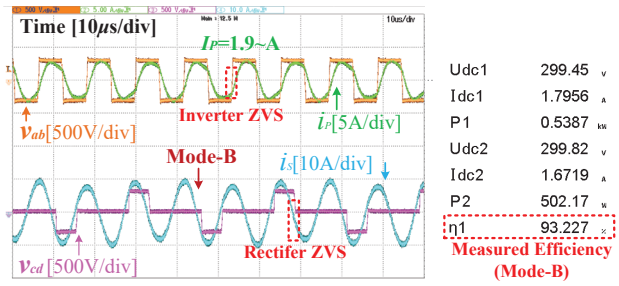

Fig. 8. Measured steady-state operating waveforms and DC-to-DC efficiency when delivering 500 W output power utilizing the proposed hybrid rectifier mode control. Here, the active rectifier is operated in mode-B.

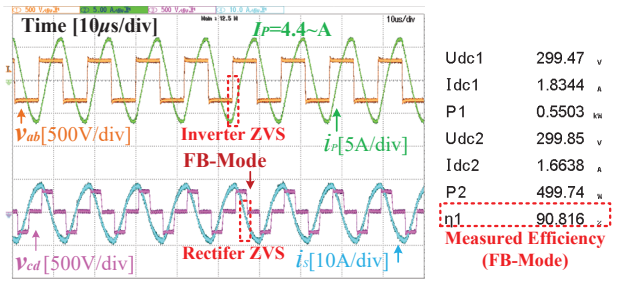

Fig. 9. Measured steady-state operating waveforms and DC-to-DC efficiency when delivering 500 W output power utilizing the conventional phase-shift control. Here, the active rectifier is operated in the FB mode.

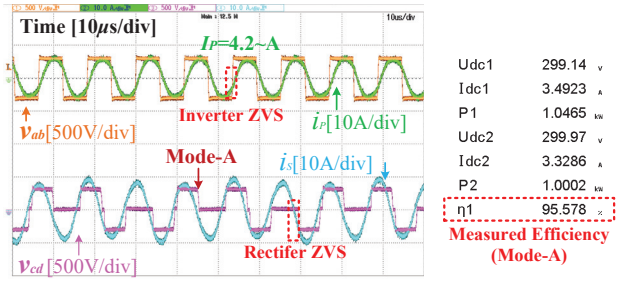

Fig. 10. Measured steady-state operating waveforms and DC-to-DC efficiency when delivering 1 kW output power utilizing the proposed hybrid rectifier mode control. Here, the active rectifier is operated in mode-A.

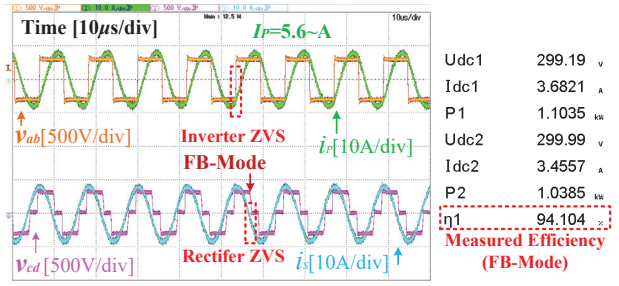

Fig. 11. Measured steady-state operating waveforms and DC-to-DC efficiency when delivering 1 kW output power utilizing the conventional phase-shift control. Here, the active rectifier is operated in the FB mode.

B. Measured Steady-state Operating Waveforms and DC-to-DC Efficiency

Fig. 8 illustrates the measured steady-state operating waveforms and DC-to-DC efficiency when delivering 500 W power under the proposed hybrid mode (mode-B). In contrast, the experimental results for the conventional full-bridge (FB) mode at the same power level are depicted in Fig. 9.

As demonstrated in Fig. 8 and Fig. 9, both the conventional FB mode and the proposed mode-B achieve ZVS for the inverter and rectifier. However, the proposed hybrid mode significantly reduces the root-mean-square (RMS) value of the Tx coil current from 4.4 A to 1.9 A, thereby considerably minimizing inverter conduction losses and Tx coil losses. Additionally, the proposed method reduces the equivalent rectifier switching times, resulting in lower rectifier switching losses. Consequently, the measured DC-to-DC efficiency is improved from 90.8% to 93.2%, demonstrating an efficiency enhancement of 2.4%.

Further comparisons at a higher power level are presented in Fig. 10 and Fig. 11, illustrating the performance when delivering 1 kW power under the proposed hybrid mode (mode-A) and the conventional FB mode.

At the 1 kW power level, although both the conventional FB mode and the proposed mode-A achieve ZVS for the inverter and rectifier, the proposed mode-A reduces the RMS value of the Tx coil current from 5.6 A to 4.2 A. This significantly decreases inverter conduction losses and Tx coil losses. Moreover, the proposed method lowers the equivalent rectifier switching times, leading to reduced rectifier switching losses. As a result, the measured DC-to-DC efficiency improves from

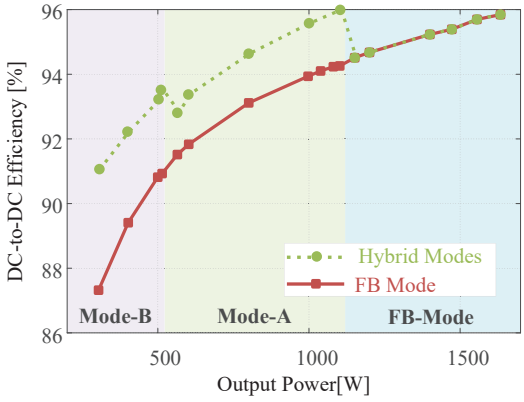

Fig. 12. Measured DC-to-DC efficiency when delivering different output power under the proposed hybrid mode control and the conventional phase-shift control. Here, the red solid line demonstrates the conventional phase-shift control strategy operating in FB mode, while the green dashed line illustrates the proposed control strategy employing hybrid rectifier modes, which include FB mode, mode-A, and mode-B.

94.1% to 95.6%, yielding an efficiency enhancement of 1.5%.

C. Overall Efficiency Optimization

Fig. 12 further illustrates the measured DC-to-DC efficiency within the entire power range when delivering different output power under the proposed hybrid mode control and the conventional phase-shift control. As it can be observed, the proposed hybrid rectifier control significantly enhances efficiency over a broad range of power levels compared to the conventional method. In contrast to the conventional phase-shift control, the proposed approach demonstrates a maximum efficiency improvement of up to 3.7%.

VI. Conclusion

In this paper, a secondary-side control strategy is implemented based on an active rectifier to enable communicationless and wide-range power regulation in WPT systems. Based on the pulse-skipping technique, two novel hybrid modes are proposed to improve the transfer efficiency of the system. These modes symmetrically distribute voltage pulses, reducing harmonic distortions and eliminating capacitor DC-blocking voltage. More importantly, the proposed hybrid modes decrease circulating reactive power within the resonant circuits and minimize the equivalent rectifier switching times. These factors contribute to reduced losses in both the converters and resonant circuits, thereby significantly improving efficiency across a broad power range. Experimental results are presented, demonstrating a significant efficiency improvement of the proposed method over the conventional phase-shift control method.

References

[1] S. Hui, "Planar wireless charging technology for portable electronic products and qi," *Proceedings of the IEEE*, vol. 101, no. 6, pp. 1290–1301, 2013.

[2] Z. Zhang, H. Pang, A. Georgiadis, and C. Cecati, "Wireless power transfer—an overview," *IEEE transactions on industrial electronics*, vol. 66, no. 2, pp. 1044–1058, 2018.

[3] S. Roy, A. W. Azad, S. Baidya, M. K. Alam, and F. Khan, "Powering solutions for biomedical sensors and implants inside the human body: A comprehensive review on energy harvesting units, energy storage, and wireless power transfer techniques," *IEEE Transactions on Power Electronics*, vol. 37, no. 10, pp. 12 237–12 263, 2022.

[4] H.-J. Kim, H. Hirayama, S. Kim, K. J. Han, R. Zhang, and J.-W. Choi, "Review of near-field wireless power and communication for biomedical applications," *IEEE Access*, vol. 5, pp. 21 264–21 285, 2017.

[5] H. Liu, X. Huang, L. Tan, J. Guo, W. Wang, C. Yan, and C. Xu, "Dynamic wireless charging for inspection robots based on decentralized energy pickup structure," *IEEE Transactions on Industrial Informatics*, vol. 14, no. 4, pp. 1786–1797, 2017.

[6] S. Li and C. C. Mi, "Wireless power transfer for electric vehicle applications," *IEEE journal of emerging and selected topics in power electronics*, vol. 3, no. 1, pp. 4–17, 2014.

[7] A. Ahmad, M. S. Alam, and R. Chabaan, "A comprehensive review of wireless charging technologies for electric vehicles," *IEEE transactions on transportation electrification*, vol. 4, no. 1, pp. 38–63, 2017.

[8] D. Patil, M. K. McDonough, J. M. Miller, B. Fahimi, and P. T. Balsara, "Wireless power transfer for vehicular applications: Overview and challenges," *IEEE Transactions on Transportation Electrification*, vol. 4, no. 1, pp. 3–37, 2017.

[9] C. C. Mi, G. Buja, S. Y. Choi, and C. T. Rim, "Modern advances in wireless power transfer systems for roadway powered electric vehicles," *IEEE Transactions on Industrial Electronics*, vol. 63, no. 10, pp. 6533–6545, 2016.

[10] W. V. Wang, D. J. Thrimawithana, and M. Neuburger, "An si mosfet-based high-power wireless ev charger with a wide zvs operating range," *IEEE Transactions on Power Electronics*, vol. 36, no. 10, pp. 11 163–11 173, 2021.

[11] M. Fu, C. Ma, and X. Zhu, "A cascaded boost–buck converter for high-efficiency wireless power transfer systems," *IEEE Transactions on industrial informatics*, vol. 10, no. 3, pp. 1972–1980, 2013.

[12] X. Dai, X. Li, Y. Li, and A. P. Hu, "Maximum efficiency tracking for wireless power transfer systems with dynamic coupling coefficient estimation," *IEEE Transactions on Power Electronics*, vol. 33, no. 6, pp. 5005–5015, 2017.

[13] Z. Zhou, L. Zhang, Z. Liu, Q. Chen, R. Long, and H. Su, "Model predictive control for the receiving-side dc–dc converter of dynamic wireless power transfer," *IEEE Transactions on Power Electronics*, vol. 35, no. 9, pp. 8985–8997, 2020.

[14] G. Yu, J. Dong, T. B. Soeiro, G. Zhu, Y. Yao, and P. Bauer, "Three-mode variable-frequency zvs modulation for four-switch buck+ boost converters with ultra-high efficiency," *IEEE Transactions on Power Electronics*, vol. 38, no. 4, pp. 4805–4819, 2022.

[15] H. Zeng, N. S. González-Santini, Y. Yu, S. Yang, and F. Z. Peng, "Harmonic burst control strategy for full-bridge series-resonant converter-based ev charging," *IEEE Transactions on Power Electronics*, vol. 32, no. 5, pp. 4064–4073, 2016.

[16] R. Mai, Y. Liu, Y. Li, P. Yue, G. Cao, and Z. He, "An active-rectifier-based maximum efficiency tracking method using an additional measurement coil for wireless power transfer," *IEEE Transactions on Power Electronics*, vol. 33, no. 1, pp. 716–728, 2017.

[17] G. Zhu, J. Dong, G. Yu, W. Shi, C. Riekerk, and P. Bauer, "Optimal multivariable control for wide output regulation and full-range efficiency optimization in lcc-lcc compensated wireless power transfer systems," *IEEE Transactions on Power Electronics*, 2024.

[18] Y. Jiang, L. Wang, J. Fang, C. Zhao, K. Wang, and Y. Wang, "A joint control with variable zvs angles for dynamic efficiency optimization in wireless power transfer system," *IEEE Transactions on Power Electronics*, vol. 35, no. 10, pp. 11 064–11 081, 2020.

[19] H. Hu, T. Cai, S. Duan, X. Zhang, J. Niu, and H. Feng, "An optimal variable frequency phase shift control strategy for zvs operation within wide power range in ipt systems," *IEEE Transactions on Power Electronics*, vol. 35, no. 5, pp. 5517–5530, 2019.

[20] X. Wang, J. Xu, M. Leng, H. Ma, and S. He, "A hybrid control strategy of lcc-s compensated wpt system for wide output voltage and zvs range with minimized reactive current," *IEEE Transactions on Industrial Electronics*, vol. 68, no. 9, pp. 7908–7920, 2020.

[21] X. Zhang, T. Cai, S. Duan, H. Feng, H. Hu, J. Niu, and C. Chen, "A control strategy for efficiency optimization and wide zvs operation range in bidirectional inductive power transfer system," *IEEE Transactions on Industrial Electronics*, vol. 66, no. 8, pp. 5958–5969, 2018.

[22] Y. Li, W. Sun, X. Zhu, and J. Hu, "A hybrid modulation control for wireless power transfer systems to improve efficiency under light-load conditions," *IEEE Transactions on Industrial Electronics*, vol. 69, no. 7, pp. 6870–6880, 2021.

[23] G. Zhu, J. Dong, W. Shi, T. B. Soeiro, J. Xu, and P. Bauer, "A mode-switching-based phase shift control for optimized efficiency and wide zvs operations in wireless power transfer systems," *IEEE Transactions on Power Electronics*, vol. 38, no. 4, pp. 5561–5575, 2022.

[24] G. Zhu, J. Dong, F. Grazian, and P. Bauer, "A parameter recognition based impedance tuning method for ss-compensated wireless power transfer systems," *IEEE Transactions on Power Electronics*, 2023.

[25] G. Zhu, J. Dong, and P. Bauer, "A dynamic frequency sweeping based parameter estimation method for wireless power transfer," in *IECON 2023-49th Annual Conference of the IEEE Industrial Electronics Society*. IEEE, 2023, pp. 1–6.

[26] W. Zhang and C. C. Mi, "Compensation topologies of high-power wireless power transfer systems," *IEEE Transactions on Vehicular Technology*, vol. 65, no. 6, pp. 4768–4778, 2015.

[27] J. Yin, D. Lin, C. K. Lee, T. Parisini, and S. Hui, "Front-end monitoring of multiple loads in wireless power transfer systems without wireless communication systems," *IEEE Transactions on Power Electronics*, vol. 31, no. 3, pp. 2510–2517, 2015.

[28] V. Yenil and S. Cetin, "An improved pulse density modulation control for secondary side controlled wireless power transfer system using lcc-s compensation," *IEEE Transactions on Industrial Electronics*, vol. 69, no. 12, pp. 12 762–12 772, 2021.